Modifying the reactivity of single Pd sites in a trimetallic Sn-Pd-Ag surface alloy: Tuning CO binding strength

Lars Mohrhusen, 1,a,§ Shengjie Zhang, 2,§ Matthew M. Montemore^{2,*}, Robert J. Madix, 3,#

- ¹ Department of Chemistry and Chemical Biology, Harvard University, Cambridge, MA 02138, USA
- ² Department of Chemical and Biomolecular Engineering, Tulane University, New Orleans, LA 70118, USA
- ³ John A. Paulson School of Engineering and Applied Sciences, Harvard University, Cambridge, MA 02138, USA
- ^a Current Affiliation: Institute of Chemistry, Carl von Ossietzky Universität Oldenburg, 26129 Oldenburg, Germany
- # deceased 05/2023.

Corresponding author

- *mmontemore@tulane.edu
- § Authors contributed equally

Abstract

Improving control over active-site reactivity is a grand challenge in catalysis. Single-atom alloys (SAAs) consisting of a reactive component doped as single atoms into a more inert host metal feature localized and well-defined active sites, but fine tuning their properties is challenging. Here, we develop a framework for tuning single-atom site reactivity by alloying in an additional inert metal, which we term an alloy-host SAA. Specifically, we created about 5% Pd single-atom sites in a Pd₃₃Ag₆₇(111) single-crystal surface, and then identified Sn based on computational screening as a suitable third metal to introduce. Subsequent experimental studies show that introducing Sn indeed modifies the electronic structure and chemical

reactivity (measured by CO desorption energies) of the Pd sites. The modifications to both the electronic structure and the CO adsorption energies are in close agreement with our calculations. These results indicate that the use of an alloy host environment to modify the reactivity of single-atom sites could allow fine-tuning of catalytic performance and boost resistance against strong-binding adsorbates such as CO.

Keywords

Alloy-host single-atom alloys, CO adsorption, heterogeneous catalysis, reactive site tuning, surface chemistry, trimetallic alloy

1. Introduction

A fundamental challenge in catalysis is to fine-tune energetics for high activity, selectivity, and resistance to poisons. Dilute alloys have shown promise towards addressing this challenge. In particular, single-atom alloy (SAA) catalysts, which consist of one (typically reactive) metal doped as isolated atoms into the surface of a second (typically inert) host metal, can exhibit both low activation barriers and weak binding of downstream reaction intermediates, in contrast to many traditional catalytically active metals. Thus, SAAs have shown quite promising catalytic performance for a variety of reactions. However, conventional SAAs comprise a finite design space, simply because the periodic table offers a limited number of metals, and most combinations are predicted to be unstable. This limits the tailoring of the reactivity of SAAs for a particular reaction. Specifically, CO poisoning is a common issue for several important processes of a particular reaction. Specifically, CO poisoning is a common issue for several sites could prove valuable for developing new catalysts.

Here, we demonstrate the possibility of tuning the properties of SAA active sites by adding a significant amount of an additional (third) metal to modify the local environment around the single-atom site. In general, this metal could modify the electronic and chemical properties of the single-atom dopant directly, or could modify the reactivity of host sites near the single-atom dopant. In this work we focus on the former,

direct modification of the single-atom dopant's properties. This relatively new class of materials, which we term "alloy-host SAAs", preserves many of the advantages of SAAs, such as: their ability to induce deviations from linear correlations between energies, [13–15] the possibility of unique electronic structure [16] or to spill over adsorbed intermediates, [17,18] and their suitability for computational modelling. [3] While a few previous studies show the effectiveness of these types of materials for specific reactions, rational design and fundamental studies are lacking. [19–24] Indeed, because of the large design space for alloy-host SAAs, computational methods are needed for efficient screening. Furthermore, surface-science techniques on well-defined, single-crystal materials bring strong insight into the structure and chemical reactivity of these materials and can provide more granular validation of computational predictions.

More broadly, many alloys with three or more components have shown promise in catalysis;^[25,26] however, most of these materials are structurally very complex and often feature a broad distribution of active sites. Alloy-host SAAs could feature more well-defined active sites than most trimetallic alloys, with the single-atom sites being more amenable to computational modelling and single-crystal studies. Indeed, we show below the possibility of distinct active sites as well as the possibility of nearly uniform active sites. Furthermore, alloy-host SAAs are distinct from dual-atom alloys (DAAs), which have been recently demonstrated, even though both are trimetallic alloys. DAAs consist of two active single-atom dopants in a heterodimer, while alloy-host SAAs consist of one active single-atom dopant surrounded by two relatively inert metals in higher concentrations.

The dilute PdAg system is an excellent platform for the development of alloy-host SAAs, since single Pd sites are readily formed from more Pd-rich starting alloys due to segregation at elevated temperatures. It was previously shown that a coverage of single Pd sites of 5-6% can be stabilized on the (111) surface of a bulk Pd₃₃Ag₆₇ single crystal, which is employed as a platform herein. [29] This material acts as a model system for e.g. selective hydrogenation catalysts, for which dilute Pd alloys have shown promising results. [1,30–34]

Thus, in this work, we first computationally screen a number of metals for modifying the reactivity of Pd single sites in a PdAg alloy single crystal, identifying Sn as an attractive candidate. Subsequent experimental studies confirm that Sn modifies both the electronic structure and chemical properties of the Pd single-sites, demonstrating a clear strategy for tuning single-site reactivity.

2. Results and Discussion

2.1 Computational screening of metals

We first used density functional theory (DFT) to screen for additional metals to modify the reactivity and local environment of single Pd sites in the PdAg alloy surface. Ideally, this additional metal should prefer to selectively coordinate to Pd, should not prefer to form clusters with itself, and should prefer the surface over the subsurface to avoid segregation into the bulk. While it may be possible to stabilize some additional metals on the surface using kinetic trapping or in the presence of adsorbed species, for experimental convenience we focused on metals that are predicted to be stable in the surface layer under vacuum. We thus screened nineteen metals for these three factors (Figure 1). We first tested whether the additional metal M prefers to lie next to Pd or away from Pd, targeting a negative M-Pd formation energy. The results indicated that most metals prefer to lie next to Pd rather than be completely surrounded by Ag atoms. Next, we tested whether each metal prefers to exist as a dimer or a monomer, where monomers are preferred to prevent clustering; that is, a positive M-M formation energy is desired. Most metals prefer to dimerize, leaving only a few promising candidates. Finally, we tested whether each metal prefers the surface or subsurface (aiming for a negative surface preference energy), and found that most metals prefer the subsurface (segregation into the bulk).

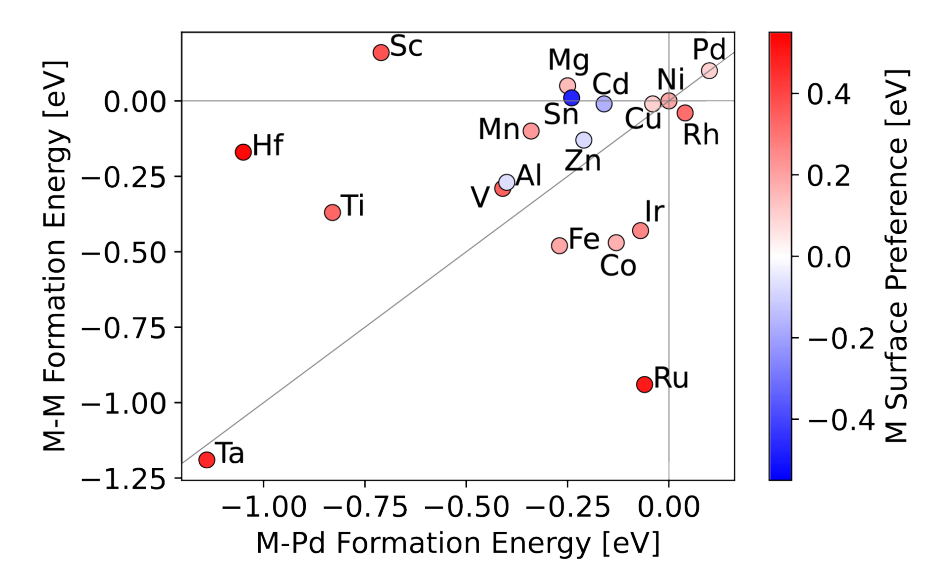


Figure 1. DFT screening of additional metals to add to a PdAg alloy to modify the local environment of the Pd sites. The M-M homodimer formation energy, M-Pd heterodimer formation energy, and surface preference (compared to subsurface) are all shown. The most promising metals will be in the upper-left region of the chart and have a blue color. For clarity, W, Re, and Mo are not shown as they feature very strong homodimer formation energies, making them poor candidates and making it difficult to read the plot.

Only one metal, Sn, completely satisfies all three criteria. As these screening criteria are calculated at low temperature, we have also performed some analysis to estimate possible temperature effects (see Supporting Information). In short, this analysis suggests that SnPdAg should be stable at reasonable temperatures that are often used in surface science and catalysis. Sn is also relatively inert towards C-containing species, which allows us to maintain the SAA paradigm of a single reactive atom (in this case, Pd) embedded in a more inert host (SnAg surface alloy). Additional calculations for the (110), (100), and (211) facets again generally indicate Sn as the most promising metal (see Figure S1 in the Supporting Information). Therefore, we chose Sn for experimental studies as it is predicted to lie next to Pd in the surface and thus could modify its electronic and chemical properties as well as changing the local chemical environment. Other metals may also be viable for tuning the Pd single-site reactivity depending on the temperature, metal loading, and

presence of adsorbed species. In particular, Cd, Zn, and Al would be expected to prefer the surface layer and prefer Pd over themselves, although they may cluster with themselves for some conditions and compositions. Cu and Mg could be effective third metals if adsorbed species were present to stabilize them in the surface layer.

2.2 Electronic modification of single Pd sites by Sn

Based on the computational results, we experimentally tested whether Pd sites in a PdAg (111) alloy surface can be electronically modified by defined coordination with Sn atoms. This effect was directly probed on surfaces with 5-6% single Pd sites embedded in the surrounding Ag (formed from a Pd₃₃Ag₆₇(111) bulk alloy by annealing to 820 K in UHV).^[29] Comprehensive experimental details can be found in the Methods Section, but for clarity the main aspects are summarized here. All experiments were performed under ultrahigh vacuum conditions using a commercial Pd₃₃Ag₆₇(111) single crystal purchased from Surface Preparation Laboratory. Upon argon ion sputtering and subsequent annealing to 820 K in UHV, a surface with 5-6 % single Pd sites surrounded by Ag atoms is formed as we and others have shown in previous work. ^[29,36-38] The surface structure, quality and cleanliness were checked by XPS, CO TPD and LEED throughout the course of experiments. This surface is used as a platform within this work. Sn (typically 0.05 – 2 ML) was deposited onto such surfaces from an electron beam evaporator at 300 K in UHV.

Figure 2 shows spectra recorded after incremental deposition of Sn on the PdAg surface at room temperature (b-d) together with a library of predicted core-level shifts from DFT for different Sn coordination around the Pd sites. Note that in all cases the full spin-orbit split doublet was considered for all experimental analyses and deconvolutions, but for clarity only the more intense component is displayed here.

From the Pd3d_{5/2} detail spectra (Figure 2b), it is evident that in addition to unmodified Pd species (peaking at 334.8 eV, grey), additional components develop with increasing Sn deposition in a shoulder towards higher binding energies, denoted as alloyed species in the following. Based on our DFT models, the

shoulder can be deconvoluted using two components. The first component accounts for Pd in low (but nonzero) Sn coordination (1-3 Sn per Pd) being shifted 0.6 eV (blue in Figure 2). This value was chosen as an average of core-level shifts predicted by DFT for different species from 1 to 3 Sn per Pd site. Merging these chemical species into one spectral component appears appropriate since CO TPD spectra (Figure 4 below) show that these three species coexist even for small Sn coverages of 0.12 ML. Furthermore, deconvolution of the Sn-modified Pd with three or more individual components was found to result in large error margins, further supporting the use of two components. The second component accounts for Pd in higher Sn coordination (4 and more Sn per Pd), being shifted by +1.1 eV (red in Figure 2), again in excellent agreement with DFT.

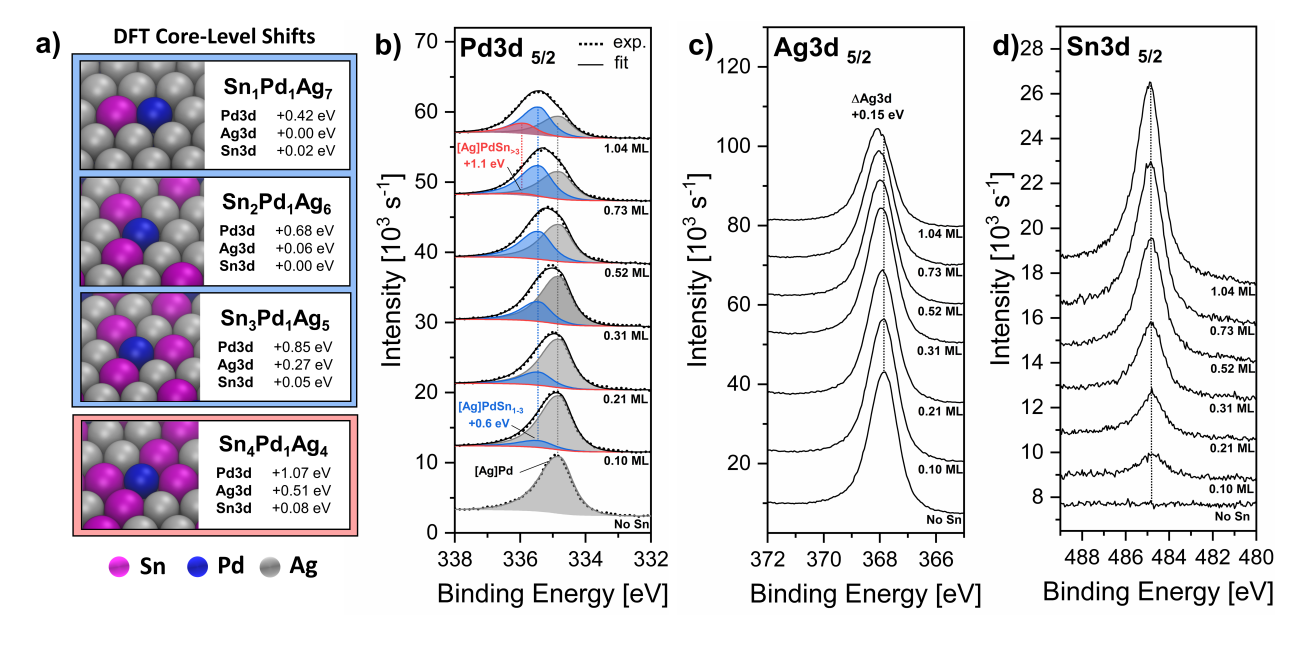


Figure 2 a) Library of DFT-calculated core level shifts for single Pd sites in a Ag surface layer with a lower (Sn₁Pd₁Ag₇, Sn₂Pd₁Ag₆, and Sn₃Pd₁Ag₅, blue) and higher (Sn₄Pd₁Ag₄, red) Sn coordination around the Pd site. b-d) XPS spectra for different coverages of Sn deposited at 300 K. b) Pd3d_{5/2} spectra. Two classes of alloy species develop at higher binding energies with ongoing Sn deposition, first for low Sn coordination (blue), later for higher Sn coordination numbers (red). c) Ag3d_{5/2} region, which shows a small

overall peak shift (up to 0.15 eV). No peak deconvolution is done here to avoid large error margins due to the relatively small peak shift. d) $\text{Sn}3d_{5/2}$ region, which also shows a very small peak shift.

For low Sn coverages (up to approx. 0.3 ML), the low-coordinated species grows while the intensity of the unmodified Pd signal decreases slightly. For higher coverages (> 0.5 ML), the alloyed species grows further and begins to dominate. Approaching even higher coverages, 0.73 ML and above, the highly Sn-coordinated alloy species forms while the low-coordinated one becomes less prevalent. Throughout, the signal of the unmodified Pd decreases with increasing coverage. Note that at room temperature the grade of alloying likely is kinetically hindered as we show at a later point. This is all consistent with the picture of an increasing Sn content in the topmost surface, causing an increasing electronic modification of the Pd sites. As expected based on the DFT calculations, the Sn3d signal grows with increasing coverage but shows no significant peak shifts (Figure 2d).

Sn was chosen because of its tendency to selectively coordinate to Pd sites, and indeed the electronic modification effect is larger on Pd than for Ag as is evident from the Ag3d lines. The Ag3d peaks decrease in intensity with increasing Sn coverage but exhibit only a very small overall shift (up to 0.15 eV for 1.04 ML of Sn). Due to this very small peak shift, a deconvolution would be subject to large errors and is thus not considered. The results are also in good agreement with the predicted core level shifts. Thus, it is clear that Sn atoms can be used to selectively modify the electronic structure of Pd sites in a Ag matrix, as predicted by our DFT calculations. We also generated simulated scanning-tunneling microscopy images with and without adsorbed CO (see Figure S2).^[39]

As seen in the calculated projected density of states (PDOS, Figure 3), these Pd single-atom sites exhibit "free-atom-like" d states. [16,28,40] After doping Sn into the surface, Pd's d bands become lower and broader, indicating interactions between Pd and Sn. Additionally, such interaction brings a downshift to the d band (more negative, away from the Fermi energy). According to d-band theory, a downshift of the d bands should result in weaker adsorption, which is consistent with our calculations and the following experiments.

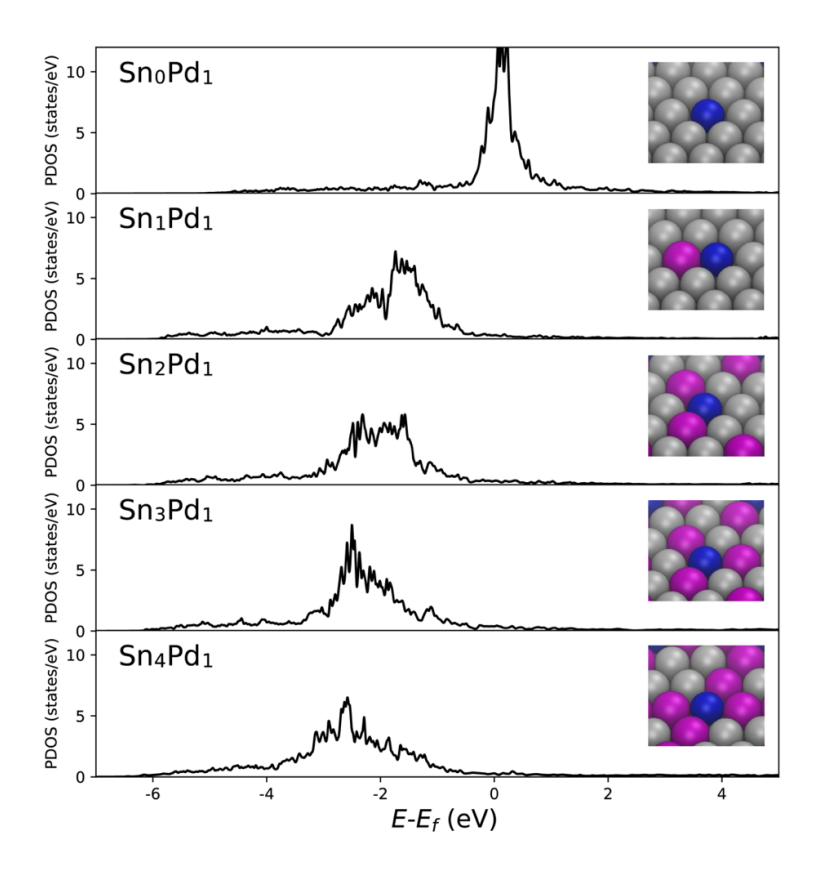


Figure 3. PDOS on a Pd atom in the alloy surface with an increasing number of Sn neighbors.

2.3 Chemical modification of single Pd sites by Sn and thermal effects

Moreover, we found the modification of Pd sites by Sn affects the molecular binding of adsorbates such as CO. Figure 4 shows temperature-programmed desorption spectra of CO (m/z = 28) acquired from the initial PdAg surface, the surface after deposition of 0.15 ML Sn at 300 K, and again after anneal to 400 K and 450 K to maximize alloying. DFT-predicted desorption temperatures (with a constant shift as explained below) for CO at single Pd sites with different Sn coordination are displayed for comparison.

While the initial PdAg surface is known to yield only one desorption feature from the Pd single sites,^[29] additional signals occur at lower temperatures when Sn is present. Based on the DFT calculations, we assign these additional peaks to desorption from single Pd sites with one, two or three adjacent Sn atoms. The DFT-predicted desorption temperatures were shifted by 50 K, as absolute values are not expected to be

quantitatively accurate. After this shift there is very close agreement between the DFT and the experiment, within approximately 5 to 15 K. Thus, the DFT calculations apparently capture the Sn-induced shifts in CO adsorption energy quite accurately and allow clear assignments of the various local environments around the Pd. Moreover, we have calculated stretching frequencies for CO adsorbed at the different Sn_xPd₁Ag adsorption sites (Table S2), as well as adsorption energies for other third metals (Table S3).

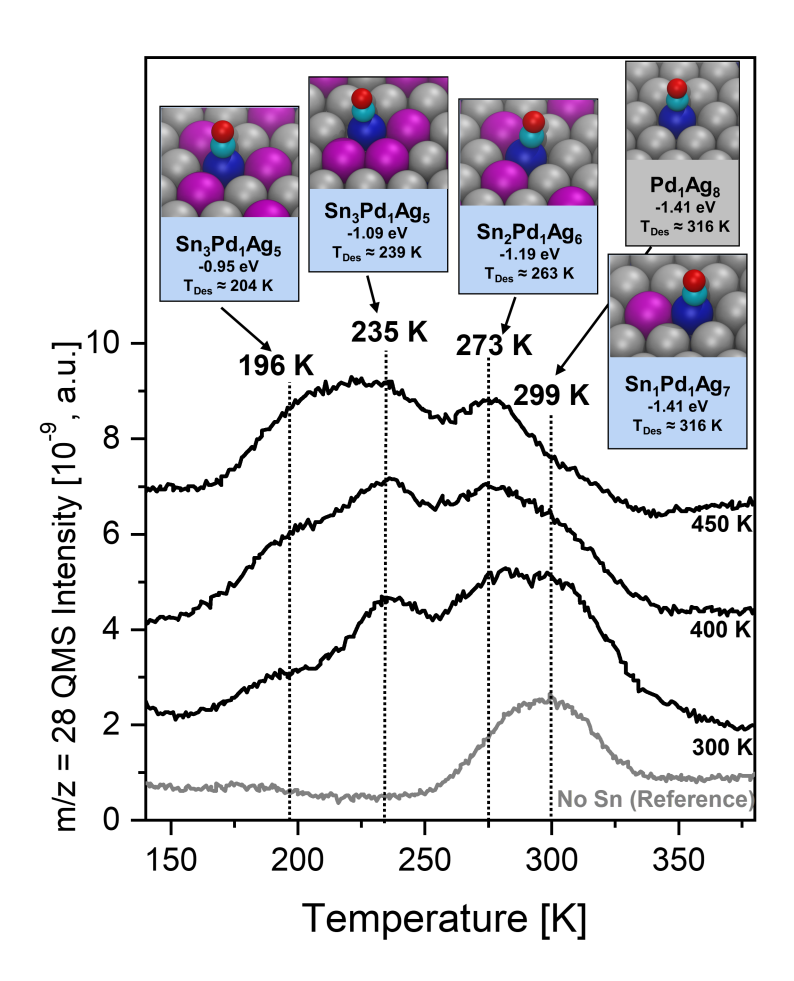


Figure 4 Thermal desorption of CO (0.03 L at 100 K) from Sn_xPd₁Ag surfaces (0.15 ML Sn at 300 K) with postannealing to 400 K and 450 K to maximize alloying. All desorption features can be attributed to desorption from single Pd sites with different Sn coordination via DFT. CO does not adsorb on Ag or Sn sites under the conditions used here.

To provide additional information on the reactivity of the surface atoms and exclude other possible surface structures, we performed calculations of CO adsorbed on Sn sites, and found that CO tends to spontaneously desorb or exhibit a positive adsorption energy on Sn monomers and larger ensembles. If there are neighboring Pd atoms, CO moves from Sn to Pd sites. Similarly, CO adsorption is quite weak on Ag, as is well known, and we calculate an adsorption energy of -0.38 eV, which would correspond to desorption around 60 K in TPD experiments, using the same TPD prediction methodology as above. The latter is in line with experimental results reporting CO desorption from Ag(111) below 60 K.^[41]

We also performed calculations to confirm that only one CO molecule can reside on the Pd site. We find that the second CO molecule has an adsorption energy of -0.50 eV, which would correspond to desorption around 92 K in TPD experiments. Again, this agrees well with a study on a PdAg (111) surface alloy with 2% Pd, on which exclusive atop CO adsorption on single Pd sites was observed via HREELS^[42,43] along with work from the group of Jason Weaver.^[38]

Finally, we performed calculations for CO adsorption on surface dimers and trimers of Pd. We find adsorption energies of -1.58 eV on a Pd dimer and -2.04 eV on a surface trimer. These would correspond to desorption around 356 and 464 K in TPD experiments. Experimental reports along with our own previous work support this finding, reporting desorption temperatures of around 360 - 400 K and around 460 K, respectively.^[29,42,43]

After deposition at 300 K, the grade of alloying—and thus the distribution of adsorption sites with specific binding energies—can be modified by mild thermal treatments. Assuming that the distribution of Sn on the surface is kinetically controlled at room temperature, annealing to 400 – 450 K seems to overcome this barrier to form more Pd₁Sn_x sites according to CO TPD (Figure 4). Given the lack of additional Sn, we suggest that Sn that was originally only coordinated to Ag gains enough mobility to form the energetically preferred Sn-Pd interactions (see 3.1). In this example, 0.15 ML of Sn were deposited onto a surface that contains 5-6% Pd sites. The intensity of the desorption species peaking at 300 K (from pristine Pd sites or

single Pd₁Sn₁ sites) is almost fully diminished after annealing to 450 K, indicating that Sn indeed preferentially coordinates to Pd instead of forming a random mixture.

A similar effect can also be observed in temperature-dependent XPS experiments after deposition of 0.15 ML Sn at room temperature (Figure 5). The percentage of the alloyed species in the Pd3d signals (Figure 5a) increases from 300 to 400 K, further increases only very little between 400 and 500 K, and then drops significantly above 550 K. This is in clear agreement with the intensity of the Sn3d lines; however, the signal-to-noise ratio at this coverage does not allow a more detailed analysis of the Sn signals. The Ag3d lines (not shown) do not exhibit significant trends, which is expected for such low Sn coverages. After annealing to 820 K, no Sn is left at the surface, and the Pd component correspondingly changes back to its original shape and position.

Additional annealing experiments indicate that the distribution of site reactivity can be controlled. After annealing to 550 or 650 K, essentially only one desorption peak is observed, which is shifted from the unmodified Pd sites. At 550 K, the peak position indicates that primarily Sn₂Pd₁Ag sites are present, with the long tail on the low-temperature side suggesting that there are also a few Pd sites with higher Sn coordination. At 650 K, there appears to be a shoulder on the high-temperature side, suggesting that there are some sites with lower Sn coordination in addition to the majority Sn₂Pd₁Ag sites. The qualitative trends between temperature-programmed desorption and XPS are in agreement, and quantitative matching between these techniques is not expected as the XPS also probes a non-negligible amount of subsurface Pd while desorption experiments only probe the surface layer.

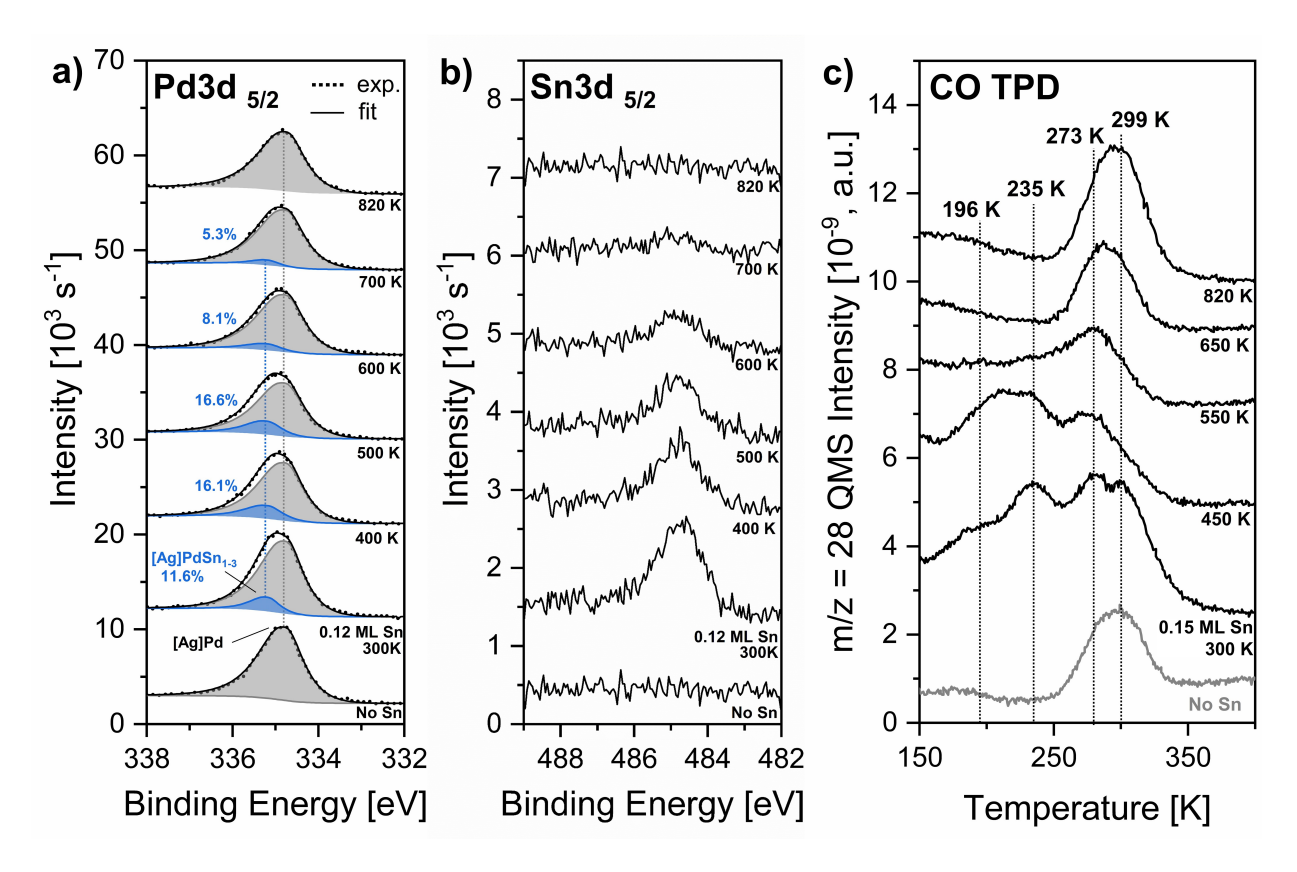


Figure 5 Overview of the thermal stability and site tunability of a Sn-Pd₁Ag surface alloy (0.12 - 0.15 ML Sn) in XPS and CO TPD. a) Pd3d _{5/2} spectra as a function of annealing temperature after deposition of 0.12 ML Sn at 300 K. The percentage of the alloyed Pd species of the overall amount of Pd is indicated in blue. b) corresponding Sn3d _{5/2} spectra. c) CO TPD spectra (0.15 ML Sn, 0.03 L at 100 K)

From the XPS and TPD results, it is clear that Sn is removed from the surface at temperatures above 650 K. Subsurface segregation or evaporation into the vacuum are the two possible explanations. No signs of Sn evaporation from the surface were observed (no signals even for high coverages (> 2ML) in the QMS trace of m/z = 120 Sn (32.6% of overall Sn due to natural isotope distribution)) during annealing, but there is clear evidence for segregation into the bulk being the relevant mechanism from emission angle-dependent XPS. In brief, a sample prepared by deposition of 0.5 ML Sn at 300 K shows an increasing overall content of Sn (total composition (Sn/(Sn+Pd+Ag)) with decreasing probing depth, indicating that most or all of the Sn is located at the topmost surface as expected. However, after annealing to 700 K for a few minutes, an

equal distribution of Sn was found within the upper few nm of the sample, which yields clear evidence for kinetically limited segregation into the bulk, which is quenched by rapid cooling to record the spectra. DFT calculations indicate an enthalpic driving force for Sn to remain in the top surface layer (see Section 3.1), and this is consistent with the fact that some Sn remains on the surface until roughly 600 K. In contrast, at higher temperatures entropy drives the Sn to the bulk of the crystal.

3. Discussion

Our work is generally consistent with previous studies of bimetallic alloys. These studies have considered Sn as the inert component for Pd-rich alloys, and have also studied the formation of a few ordered surface reconstructions on the Pd(111) surface (especially $\sqrt{3} \times \sqrt{3}$ R30° and p(2×2)). [44-46] In accordance with our findings, an electronic interaction between the Pd and the Sn sites has been identified based on Pd3d XPS and CO TPD. While a similar trend towards lower CO desorption temperatures (shifted from around 420 K to around 370 K) was observed by Lee et al., that study revealed a shift in the Pd3d signals in the opposite direction than observed in this study. Also, in that study a shift of the Sn3d in the same direction was reported, which was absent herein. However, while the chemistry of PdSn(111) surface alloys is generally dominated by the occurrence of the ordered superstructures, such superstructures were not observed for any of our trimetallic alloy-host SAAs (see Figure S5), underlining the different behavior of bulk Pd and single Pd sites surrounded by another metallic host.

Likewise, intermetallic bulk phases have been reported such as Pd₃Sn₂, Pd₂Sn or PdSn. Interestingly, these phases can exhibit different chemical selectivities, for example in hydrogenation of unsaturated ketones such as crotonaldehyde. Orthorhombic PdSn for example has a high selectivity towards the unsaturated alcohol, while others yield the expected saturated ketone.^[47] Ag₃Sn also exhibits an ordered phase that is different from Ag or PdAg.^[48] All of these phases can be easily distinguished by their crystal diffraction patterns. In this work, no signs of any structural change to the crystal bulk have been observed. Similarly, no evidence for Sn-induced strain was found. However, for small alloy nanoparticles on supports, which

have an intrinsically smaller bulk volume, both of these factors may impact the formation and properties of bulk and surface sites, depending on the overall composition.

Given the similarity of Pt and Pd, there are some reports for PtSn alloys from single crystal experiments to supported nanoparticles. These studies^[49–52] find that the CO binding to Pt sites can be weakened by mixing Sn into the Pt surface via TPD-, IR- and high-resolution ARPES experiments. All three conclude that the Sn coordination modifies the d-band of the Pt surface and thus weakens the π bonding of adsorbed CO. Nevertheless, in all cases the authors state that distinct surface reconstructions (again $\sqrt{3} \times \sqrt{3}$ R30° and 2×2) dominate the surface chemistry. Another report presents the weakened CO binding on a Sn/Ni(111) with the same surface reconstructions.^[53] However, all the observations on the electronic structure (d-band effect) and weakening of the CO binding are in good agreement with the observations herein and show that such concepts may be translated to alloy-host SAAs.

4. Conclusion

Modifying the reactivity of single-atom sites in alloys could allow fine tuning for high catalytic performance, such as lessening CO poisoning by weakening the binding of CO. Here, we created Pd single-atom sites in a single-crystal PdAg alloy surface and used computational screening to identify an additional metal to add in order to modify the Pd sites. Sn was predicted to prefer the surface and to prefer to coordinate selectively to Pd, without forming large Sn clusters. Thus, Sn was experimentally added to the PdAg surface, and XPS and TPD showed that the Sn coordination modifies the electronic structure and chemical reactivity (in terms of CO binding) of the Pd sites. These modifications are in close agreement with computational predictions, indicating that the computational models are a good representation of the experimental active sites, which is difficult to achieve for most alloys with three or more components. Tuning the annealing temperature allowed some control over the local environment of the Pd sites and their reactivity. In particular, annealing to 450 -550 K resulted in Pd sites with relatively uniform chemical reactivity, giving a single CO desorption peak at significantly lower temperatures than the Sn-free surface.

These fundamental studies could inform rationally designed tuning of single-atom sites in nanostructured catalysts.

5. Methods

5.1 Experimental Details

X-ray photoelectron spectroscopy (XPS), low-energy electron diffraction (LEED), and temperature-programmed desorption experiments were performed in an ultrahigh vacuum (UHV) system consisting of an analysis chamber (base pressure $\sim 2 \times 10^{-10}$ Torr) and a preparation chamber (base pressure $\sim 4 \times 10^{-10}$ Torr) described in further detail elsewhere.^[54]

The PdAg(111) sample (Surface Preparation Laboratory) was cleaned by repeated cycles of Ar⁺ sputtering (100 K, 15-20 min, 2 keV, \approx 4-5 μ A) and annealing in UHV at 820 K (typically 10-15 minutes). This yields surfaces with 5-6% single Pd sites embedded in the surrounding Ag.^[29] The surface cleanliness and order were frequently checked with XPS and LEED. The bulk stoichiometry of the sample was determined previously by normal emission XPS and energy-dispersive X-ray spectroscopy (EDS) to be 33% Pd and 67% Ag.^[55] The temperature was measured with a K-type thermocouple placed in a pinhole on the unpolished edge of the sample. Sample cooling was accomplished through direct thermal contact of the sample to a liquid nitrogen source.

Sn was evaporated onto the sample at 300 K from Sn pellets (Kurt J. Lesker, 99.998-99.999% purity) from a Ta crucible mounted in a Focus EFM electron beam evaporator (≈13 W, leading to ≈0.036 ML min⁻¹). The deposition rate was determined from a 10-step deposition series between by XPS.^[54,57,57,58] Where applicable, the sample was postannealed to the given temperatures in UHV for 10 minutes.

The total amount of Sn added throughout the course of experiments was some tens of monolayers at most. Due to Sn segregation into the bulk, an extremely small amount of Sn is likely captured in the sample (estimated below ≈ 0.0005 at%). No signs of any structural changes of the bulk sample have been observed via electron diffraction (LEED; Figure S5). Also, after standard surface cleaning, Sn contaminants were not detected by XPS, CO TDS or LEED in any of the experiments.

During the course of experiments, no evidence was found for the formation of any long-range ordered surface structures or intermetallic phases involving Sn. With low energy electron diffraction (LEED, see Figure S5), the 1×1 surface reconstruction of the (111) PdAg surface was confirmed. Upon deposition of Sn at room temperature, the reflexes are blurred, indicating the absence of any ordered superstructure implying a random distribution, as random as the Pd single site distribution. Upon annealing, the initial 1×1 (111) pattern became more and more visible, especially when Sn segregates into the bulk above 500-550 K. Thus, we exclude that ordered superstructures or intermetallic phases play a relevant role herein.

XPS experiments were performed using non-monochromated Al K α radiation (Perkin Elmer 04-548/32-095 with RBD 20-042) and a hemispherical analyzer (SPECS Phoibos 100 equipped with a 5-channel electron multiplier, typically 0.05 eV energy step size, 15 eV pass energy). To enhance the surface sensitivity, spectra were collected at an emission angle of $(65 \pm 8)^{\circ}$ with respect to the sample normal (information depth is estimated at 1.8 - 1.9 nm or roughly 8 atomic layers) if not stated otherwise. The Fermi edge was used for energy calibration. Photoelectron spectra were processed using Shirley backgrounds and Gauss-Lorentzian peak shapes in CasaXPS 2.3.15.^[58,59]

Carbon monoxide (Airgas, 99.997%) was used without further purification and dosed at a sample temperature of 100 K. Mass spectrometry data were collected during temperature-programmed heating with a quadrupole mass spectrometer (Hiden Hal201) at a heating rate of 1.5 K s⁻¹. The sample was placed in direct line of sight of the aperture of the spectrometer shroud while the sample heating filament was blocked by the sample itself and hence not in direct line of sight. Experiments with low coverages of CO (0.03 L at 100 K) were qualitatively confirmed with higher CO doses (> 3L at 100 K) to ensure population of all relevant adsorption sites.

5.2 Computational Details

The Vienna Ab initio Simulation Package (VASP)^[60,61] was employed to conduct all of the periodic, plane-wave density functional theory (DFT) calculations in this study. The exchange-correlation functional used was the Perdew–Burke–Ernzerhof generalized gradient approximation (GGA-PBE),^[62] with the Tkatchenko–Scheffler method^[63] applied for van der Waals interactions. The cutoff energy was set to 400 eV, and a $7 \times 7 \times 1$ Monkhorst–Pack k-point mesh was utilized for relaxation calculations.

In this work, we modeled FCC(111) slabs using four layers. The surface layer was composed of Pd, Ag, and a third metal (Sn for most calculations) while the bulk was made of Pd₁Ag₂. For each layer, 3×3 unit cells were used. During relaxation calculations, the top two layers and the adsorbates were fully relaxed, while the bottom two layers remained fixed. A vacuum gap of approximately 15 Å was set along the surface normal direction.

The core-level binding energies were calculated using the Janak-Slater^[64] transition state method, consisting of 0.5 electrons excited. For Pd, Ag and Sn core-level shifts calculated in this work, surface layers of Pd₁Ag₈, Ag₉ and Sn₁Ag₈ were used as the reference states for Pd, Ag, and Sn, respectively. The CO adsorption energy E_{ads} was calculated as:

$$E_{ads} = E_{tot} - E_{surf} - E_{CO} (1)$$

where E_{tot} is the total energy with CO adsorbed on the surface, E_{surf} is the energy of the clean surface, and E_{CO} is the energy of CO in the gas phase.

Supporting Information

Analysis of entropy-driven restructuring of Sn in SnPdAg; Figure S1: Screening of third metal for the (100), (110) and (211) facets; Comparison of Janak-Slater and initial-state approximation. Figure S2: Simulated STM images with and without adsorbed CO; Figure S3: Emission angle-dependent XPS of 0.5 ML Sn on PdAg after deposition at 300 K and anneal to 700 K to probe the near-surface distribution. Figure S4: Mass spectrometry traces of Sn on PdAg to exclude a possible evaporation of Sn into the vacuum. Figure S5: LEED Patterns for 1 ML of Sn on PdAg for annealing temperatures between 300 K and 820 K.

Acknowledgements

The authors acknowledge Cynthia M. Friend for her support within this project. Suriya Ramasubramanian, Rajib Das, Connor Pope and Jason F. Weaver are acknowledged for helpful additional information about the PdAg surface structure before Sn deposition. This work was supported primarily as part of the Integrated Mesoscale Architectures for Sustainable Catalysis, an Energy Frontier Research Center funded by the US Department of Energy, Office of Science, Basic Energy Sciences under Award No. DE-SC0012573, and also by the National Science Foundation through grant CBET-2340356.

Conflict of Interest

The authors declare no competing interests.

References

- [1] M. Luneau, J. S. Lim, D. A. Patel, E. C. H. Sykes, C. M. Friend, P. Sautet, *Chem Rev* **2020**, 120, 12834.
- [2] J. D. Lee, J. B. Miller, A. V. Shneidman, L. Sun, J. F. Weaver, J. Aizenberg, J. Biener, J. A. Boscoboinik, A. C. Foucher, A. I. Frenkel, J. E. S. van der Hoeven, B. Kozinsky, N. Marcella, M. M. Montemore, H. T. Ngan, C. R. O'Connor, C. J. Owen, D. J. Stacchiola, E. A. Stach, R. J. Madix, P. Sautet, C. M. Friend, *Chem Rev* 2022, 122, 8758.

- [3] R. T. Hannagan, G. Giannakakis, M. Flytzani-Stephanopoulos, E. C. H. Sykes, *Chem Rev* **2020**, *120*, 12044.
- [4] J. Liu, M. B. Uhlman, M. M. Montemore, A. Trimpalis, G. Giannakakis, J. Shan, S. Cao, R.
 T. Hannagan, E. C. H. Sykes, M. Flytzani-Stephanopoulos, ACS Catal 2019, 9, 8757.
- [5] Y. Qi, B. Wang, M. Fan, D. Li, R. Zhang, Chem Eng Sci 2021, 243, 116786.
- [6] J. Liu, J. Shan, F. R. Lucci, S. Cao, E. C. H. Sykes, M. Flytzani-Stephanopoulos, *Catal Sci Technol* **2017**, *7*, 4276.
- [7] E. C. Wegener, B. C. Bukowski, D. Yang, Z. Wu, A. J. Kropf, W. N. Delgass, J. Greeley, G. Zhang, J. T. Miller, *ChemCatChem* **2020**, *12*, 1325.
- [8] K. K. Rao, Q. K. Do, K. Pham, D. Maiti, L. C. Grabow, *Top Catal* **2020**, *63*, 728.
- [9] C. P. O'Brien, I. C. Lee, J Phys Chem C **2017**, 121, 16864.
- [10] H. X. Zhang, S. H. Wang, K. Jiang, T. André, W. Bin Cai, *J Power Sources* **2012**, *199*, 165.
- [11] M. G. T. Burrows, W. H. Stockmeyer, David Leonard Chapman, *Proc R Soc Lond A* **1940**, 176, 474.
- [12] D. Pope, D.S. Walker, R.L. Moss, *J Catal* **1973**, *28*, 46.
- [13] M. T. Darby, M. Stamatakis, A. Michaelides, E. C. H. Sykes, *J Phys Chem Lett* **2018**, *9*, 5636.
- [14] M. M. Montemore, J. W. Medlin, *Catal Sci Technol* **2014**, *4*, 3748.
- [15] M. M. Montemore, J. W. Medlin, J Phys Chem C **2013**, 117, 20078.
- [16] M. T. Greiner, T. E. Jones, S. Beeg, L. Zwiener, M. Scherzer, F. Girgsdies, S. Piccinin, M. Armbrüster, A. Knop-Gericke, R. Schlögl, Nat Chem 2018, 10, 1008.
- [17] F. R. Lucci, M. T. Darby, M. F. G. Mattera, C. J. Ivimey, A. J. Therrien, A. Michaelides, M. Stamatakis, E. C. H. Sykes, *J Phys Chem Letters* **2016**, *7*, 480.
- [18] C. R. O'Connor, K. Duanmu, D. A. Patel, E. Muramoto, M. A. van Spronsen, D. Stacchiola,
 E. C. H. Sykes, P. Sautet, R. J. Madix, C. M. Friend, *Proc Nat Acad Sci* 2020, *117*, 22657.

- [19] T. Chao, X. Luo, W. Chen, B. Jiang, J. Ge, Y. Lin, G. Wu, X. Wang, Y. Hu, Z. Zhuang, Y. Wu,X. Hong, Y. Li, *Angew Chem Int Ed* 2017, 56, 16047.
- [20] P. Mukherjee, I. M. Patil, M. Lokanathan, H. Parse, B. Kakade, A. Swami, *J Alloys Compd* **2022**, *918*, 165520.
- [21] Y. Yao, S. Hu, W. Chen, Z.-Q. Huang, W. Wei, T. Yao, R. Liu, K. Zang, X. Wang, G. Wu, W. Yuan, T. Yuan, B. Zhu, W. Liu, Z. Li, D. He, Z. Xue, Y. Wang, X. Zheng, J. Dong, C.-R. Chang, Y. Chen, X. Hong, J. Luo, S. Wei, W.-X. Li, P. Strasser, Y. Wu, Y. Li, *Nat Catal* **2019**, 2, 304.
- [22] Y. Zhu, J. Peng, X. Zhu, L. Bu, Q. Shao, C. W. Pao, Z. Hu, Y. Li, J. Wu, X. Huang, *Nano Lett* **2021**, *21*, 6625.
- [23] T. Yamada, T. Kojima, E. Abe, S. Kameoka, Y. Murakami, P. Gille, A. P. Tsai, *J Am Chem Soc* **2018**, *140*, 3838.
- [24] T. Yang, F. Qin, S. Zhang, H. Rong, W. Chen, J. Zhang, *Chem Comm* **2021**, *57*, 2164.
- [25] J. W. M. Crawley, I. E. Gow, N. Lawes, I. Kowalec, L. Kabalan, C. R. A. Catlow, A. J. Logsdail, S. H. Taylor, N. F. Dummer, G. J. Hutchings, *Chem Rev* 2022, 122, 6795.
- [26] Y. Xin, S. Li, Y. Qian, W. Zhu, H. Yuan, P. Jiang, R. Guo, L. Wang, ACS Catal 2020, 10,11280.
- [27] P. L. Kress, S. Zhang, Y. Wang, V. Çınar, C. M. Friend, E. C. H. Sykes, M. M. Montemore, *J Am Chem Soc* **2022**, 145, 8401-8407
- [28] S. Zhang, E. C. H. Sykes, M. M. Montemore, *Chem Sci* **2022**, *13*, 14070.
- [29] L. Mohrhusen, T. Egle, J. D. Lee, C. M. Friend, R. J. Madix, J Phys Chem C 2022, 126, 20332.
- [30] A. Filie, T. Shirman, A. C. Foucher, E. A. Stach, M. Aizenberg, J. Aizenberg, C. M. Friend,R. J. Madix, J Catal 2021, 404, 943.
- [31] J. E. S. Van Der Hoeven, H. T. Ngan, A. Taylor, N. M. Eagan, J. Aizenberg, P. Sautet, R. J. Madix, C. M. Friend, *ACS Catal* **2021**, *11*, 6971.

- [32] M. Luneau, E. Guan, W. Chen, A. C. Foucher, N. Marcella, T. Shirman, D. M. A. Verbart, J. Aizenberg, M. Aizenberg, E. A. Stach, R. J. Madix, A. I. Frenkel, C. M. Friend, *Commun Chem* **2020**, *3*, 1.
- [33] M. Luneau, T. Shirman, A. Filie, J. Timoshenko, W. Chen, A. Trimpalis, M. Flytzani-Stephanopoulos, E. Kaxiras, A. I. Frenkel, J. Aizenberg, C. M. Friend, R. J. Madix, *Chem Mat* 2019, 31, 5759.
- [34] M. Luneau, T. Shirman, A. C. Foucher, K. Duanmu, D. M. A. Verbart, P. Sautet, E. A. Stach, J. Aizenberg, R. J. Madix, C. M. Friend, ACS Catal 2020, 10, 441.
- [35] G. O. Kayode, M. M. Montemore, J Mater Chem A Mater 2021, 9, 22325.
- [36] P. T. Wouda, M. Schmid, B. E. Nieuwenhuys, P. Varga, Surf Sci 1998, 417, 292.
- [37] T. Egle, T. J. Cavanaugh, C. M. Friend, Surf Sci 2022, 122048.
- [38] J. F. Weaver, Private Communication
- [39] J. Tersoff, D. R. Hamann, *Phys Rev B* **1985**, *31*, 805.
- [40] H. Thirumalai, J. R. Kitchin, *Top Catal* **2018**, *61*, 462.
- [41] W. Hansen, M. Bertolo, K. Jacobi, Surf Sci 1991, 253, 1.
- [42] Y. Ma, J. Bansmann, T. Diemant, R. J. Behm, Surf Sci 2009, 603, 1046.
- [43] Y. Ma, T. Diemant, J. Bansmann, R. J. Behm, *Phys Chem Chem Phys* **2011**, *13*, 10741.
- [44] A. F. Lee, C. J. Baddeley, M. S. Tikhov, R. M. Lambert, Surf Sci 1997, 373, 195.
- [45] G. Hamm, T. Schmidt, J. Breitbach, D. Franke, C. Becker, K. Wandelt, *Surf Sci* **2004**, *562*, 170.
- [46] J. Zhao, S. Zha, R. Mu, Z. J. Zhao, J. Gong, J Phys Chem C 2018, 122, 6005.
- [47] M. Chen, Y. Yan, M. Gebre, C. Ordonez, F. Liu, L. Qi, A. Lamkins, D. Jing, K. Dolge, B. Zhang, P. Heintz, D. P. Shoemaker, B. Wang, W. Huang, Angew Chem Int Ed 2021, 60, 18309.
- [48] P.-Y. Chevalier, *Thermochim Acta* **1988**, 136, 45.
- [49] C. Xu, B. E. Koel, Surf Sci 1994, 304, L505.

- [50] Q. Wang, D. Tichit, F. Meunier, H. Guesmi, *J Phys Chem C* **2020**, *124*, 9979.
- [51] A. Moscu, Y. Schuurman, L. Veyre, C. Thieuleux, F. Meunier, *Chem Comm* **2014**, *50*, 8590.
- [52] J. Jung, S. Kang, L. Nicolaï, J. Hong, J. Minár, I. Song, W. Kyung, S. Cho, B. Kim, J. D. Denlinger, F. J. Cadete Santos Aires, E. Ehret, P. Ross, J. Shim, S. Nemšák, D. Noh, S. Han, C. Kim, B. S. Mun, ACS Catal 2022, 12, 219.
- [53] C. Xu, B. E. Koel, Surf Sci 1995, 327, 38.
- [54] M. A. Van Spronsen, K. Daunmu, C. R. O'Connor, T. Egle, H. Kersell, J. Oliver-Meseguer,
 M. B. Salmeron, R. J. Madix, P. Sautet, C. M. Friend, J Phys Chem C 2019, 123, 8312.
- [55] T. Egle, T. J. Cavanaugh, C. M. Friend, Surf Sci 2022, 122048.
- [56] J. J. Yeh, I. Lindau, Atomic Data and Nuclear Data Tables 1985, 32, 1-155.
- [57] H. Shinotsuka, S. Tanuma, C. J. Powell, D. R. Penn, Surf Interf Anal 2015, 47, 871.
- [58] D. A. Shirley, *Phys Rev B* **1972**, *5*, 4709.
- [59] N. Fairley, CasaXPS Manual 2.3.15 Rev. 1.2, Casa Software Ltd., Devon, 2009.
- [60] G. Kresse, J. Hafner, *Phys Rev B* **1993**, *47*, 558.
- [61] G. Kresse, J. Furthmüller, Comput Mater Sci 1996, 6, 15.
- [62] J. P. Perdew, K. Burke, M. Ernzerhof, *Phys Rev Lett* **1996**, *77*, 3865.
- [63] A. Tkatchenko, M. Scheffler, *Phys Rev Lett* **2009**, *102*, 073005
- [64] J. F. Janak, *Phys Rev B* **1978**, *18*, 7165.